J. of Supercritical Fluids 55 (2010) 479–484

Contents lists available at ScienceDirect

The Journal of Supercritical Fluids

journal homepage: www.elsevier.com/locate/supflu

Modeling solubility in supercritical fluids via the virial equation of state

Andrew J. Schultz*, Katherine R.S. Shaul, Shu Yang, David A. Kofke

Department of Chemical and Biological Engineering, University at Buffalo, The State University of New York, Buffalo, NY 14260-4200, United States

ARTICLE INFO

Article history:
Received 17 June 2010
Received in revised form 18 October 2010
Accepted 19 October 2010

Keywords:
Mayer sampling
Supercritical mixture
Vapor–liquid equilibrium
Virial coefficient

ABSTRACT

We examine the utility of the virial equation of state (VEOS) for the prediction of the solubility of hexane in supercritical carbon dioxide. We computed virial coefficients up to fourth-order for this mixture at 353.15 K, using Mayer-sampling Monte Carlo applied to established molecular models for carbon dioxide and hexane. At this temperature, neither the third- nor fourth-order VEOS indicate the presence of a critical point for the mixture. However, the VEOS coupled with an ideal-solution treatment for the coexisting subcritical fluid phase (with parameters determined from coexistence data at one pressure) reproduces much of the solubility curve as previously established by Gibbs-ensemble molecular simulation. Comparison of the third- and fourth-order VEOS indicate that the virial treatment is converged at the conditions where it is applied.

1. Introduction

Many modeling approaches have been examined to quantify and predict the behavior of supercritical fluids and their mixtures. Joslin et al. [1] presented a brief but comprehensive survey of these methods, summarizing the strengths and weakness of each. Such techniques include empirical engineering models (e.g. cubic equations of state), molecular simulations in various ensembles, integral equation methods, lattice models, and perturbation theory. Joslin et al. considered in detail the capabilities of another type of approach, one modeling the supercritical phase with a virial equation of state (VEOS), using parameters determined directly from a molecular model. The VEOS for a binary mixture of species 1 and 2 gives the pressure P as a series in the molar density ρ

$$\frac{P}{RT} = \rho + \sum_{n=2}^{\infty} \left(\sum_{i=0,j=n-i}^{n} \frac{n!}{i!j!} B_{ij}(T) y_1^i y_2^j \right) \rho^n \quad (1)$$

where T is the temperature and R is the gas constant. The mixture virial coefficients B_{ij} depend upon the temperature but are independent of mole fractions y_i, as indicated. We refer to the expression contained in the parentheses as B_n, analogous to the VEOS for a pure fluid. We use VEOSn to represent the VEOS truncated after the nth-order term.

The VEOS has not been widely considered as a tool for describing supercritical fluid phenomena. This is largely because there has, until recently, been no feasible way to determine the virial coefficients that are input to the treatment, without perhaps fitting to experimental data. A requirement to fit to experiment before the model can be used diminishes the predictive capabilities that represent one of the strengths of the approach; moreover, it is not really feasible to measure all the relevant coefficients experimentally, except as a correlative exercise which disconnects them from their physical meaning. The practical limit for pure substances is reached at B_2 or B_3, and the additional coefficients that arise for mixtures introduce even further difficulty. Alternatives might involve application of correlations or appeals to corresponding states. However, the real value of the VEOS is that the parameters that enter into the model can be expressed rigorously in terms of the interactions of the molecules present in the system. This feature provides a route to develop the thermodynamic model from molecular considerations, perhaps (someday) even from first-principles computational chemistry. It also provides a sound basis for developing qualitative understanding of complex behaviors, such as the mechanisms underlying co-solvent effects.

Traditionally, the connection between molecular models and thermodynamic behaviors is made by molecular simulation, but these methods have drawbacks that constrain their use in practical design calculations. First, they are time-consuming to conduct, especially for state conditions near criticality where density fluctuations necessitate the use of very large simulation volumes. The calculations are even more difficult [2–6] when values of free-energy, entropy, or chemical potential are desired (which is usually the case, as these are needed for solubility calculations). Furthermore, once a bulk simulation is completed, one is left with information that is akin to experimental data, which must then be fit or modeled thermodynamically before it can be used for an engineering design calculation. In contrast, once the virial coefficients are in hand, a VEOS model can be evaluated very rapidly and, obvi-

* Corresponding author. Tel.: +1 716 645 1186; fax: +1 716 645 3822.
E-mail address: ajs42@buffalo.edu (A.J. Schultz).

0896-8446/$ – see front matter © 2010 Elsevier B.V. All rights reserved.
doi:10.1016/j.supflu.2010.10.042

ously, it presents an equation (as opposed to discrete data) that can be manipulated and used in design and optimization. Thus, the VEOS has promise to alleviate many of the drawbacks of traditional molecular simulation while keeping its primary advantage of connecting to molecular properties. Its major limitation is its inapplicability to condensed subcritical phases, which can hamper use in applications that need to characterize both subcritical and supercritical phases, ideally using a single model.

As detailed by Harvey [7], Perkins first applied VEOS2 to model supercritical solubility in 1937. Specifically, Perkins was interested in the equilibrium concentrations of ammonia in two phases: solid barium chloride octammine and a noble gas [8]. Ultimately, his B_2 values were fit empirically, but the fitting procedure was facilitated by the definition of the components of B_2 in terms of two-body integrals (sometimes referred to as "cluster integrals"). Higher-order B_n likewise can be expressed as sums of integrals over n molecules, with the number of integrals growing rapidly with n [9], and each one representing (in the case of atomic models) roughly a $3(n-1)$-dimensional integration. Thus, it is not surprising that the efforts of Perkins and others were constrained to low order and to systems of spherically symmetric models. In 1953, Ewald et al. [10] applied VEOS3 to a variety of binary supercritical mixtures, with B_2 and B_3 computed from cluster integrals using Lennard-Jones type potentials. The coefficient B_4 contains cluster integrals having six dimensions for spherically symmetric models like Lennard-Jones, which is likely why it was not until 1997 that VEOS4 was applied to supercritical mixtures, by Joslin et al. [1]. Joslin et al. considered binary and ternary mixtures of Lennard-Jones spheres, parameterized as much as possible to represent CO_2, benzoic acid, methanol, naphthalene, and acetone. They computed the required virial coefficients using painstaking quadrature methods to handle the high-dimensional integrals that appear. They show that the effort is worthwhile however, finding that VEOS4 provides a useful characterization of the properties of the Lennard-Jones mixtures they studied. The consensus from their work and others [11–14] is that VEOS4, at least for non-polar molecules, captures behaviors up to densities encompassing the critical point, and beyond (especially at higher temperature).

The primary obstacle to the realization of this molecular-thermodynamic modeling approach (apart from the separate problem of developing a description of the coexisting subcritical phase) is the difficulty of calculating the virial coefficients for a given molecular model. More generally, this problem has long restricted the VEOS to applications at the low densities and high temperatures where unobtainable high-order coefficients are unimportant. The quadrature methods used by Joslin et al. become untenable in application to multi-atomic molecules, which introduce the need to integrate over orientational and (for non-rigid molecules) conformational degrees of freedom. As a remedy, Tomberli et al. considered a virial-based approach in which the coefficients are given via corresponding states [11] or a group-contribution scheme [15]. Ideally, however, the best predictive ability should be expected from direct calculation of the coefficients from a detailed molecular model. The introduction of the Mayer-sampling Monte Carlo (MSMC) method [16] now permits calculation of higher-order B_n. Applications to date include calculation of coefficients up to B_8 for the Lennard-Jones potential [12], B_6 for a series of Lennard-Jones mixtures [17], B_6 for a variety of water models [18–21], B_6 for alkanes [22], and B_4 for methanol [23].

The remaining concern with regard to the VEOS is that it is formed as a series expansion in density, and consequently it will begin to fail at sufficiently high density and/or low temperature. The degree to which this is a problem, however, is largely unexplored. We seek to better characterize the convergence behavior of the VEOS in the supercritical region, as well as to demonstrate that the VEOS can now be applied to mixtures with realistic molecular models through application of MSMC methods for computing the virial coefficients. We begin with a simple exercise in Section 2.1, in which we apply the VEOS to the van der Waals and Soave-Redlich Kwong equations of state for the sole purpose of characterizing the convergence of the virial series. In the remainder of this work, we consider the solubility of hexane in CO_2, employing realistic molecular models of each to compute the mixture virial coefficients. In subsequent parts of Section 2, we describe the molecular models and briefly describe the methods used to calculate the virial coefficients for these. Then, in Section 3, we present and discuss properties computed from the resulting VEOS before concluding in Section 4.

2. Models and methods

2.1. VEOS estimates of model van der Waals and Soave-Redlich-Kwong binary mixtures

Harvey [7] considered the suitability of the VEOS for application to supercritical solubility by examining VEOS3 approximations to several cubic equations of state, including the van der Waals (vdW) equation of state and the Soave-Redlich-Kwong (SRK) equation of state, for mixtures of carbon dioxide with either benzene, naphthalene, or anthracene. Now that it is feasible to use higher-order molecular-based VEOSn, it is worthwhile to briefly extend Harvey's analysis. In particular, we consider formulations up to VEOS7 applied to mixtures defined by the vdW equation of state (in the spirit of this special issue), as well as the more realistic SRK equation of state, examining benzene dissolved in carbon dioxide, and hexane dissolved in carbon dioxide.

Similar to Harvey, we first consider the vdW equation of state

$$Z \equiv \frac{P}{\rho RT} = \frac{1}{1-b\rho} - \frac{a\rho}{RT} \tag{2}$$

for a binary mixture, with Lorentz–Berthelot mixing rules for the vdW parameters a and b given in terms of the pure-component parameters a_i and b_i

$$a = y_1^2 a_1 + 2y_1 y_2 \sqrt{a_1 a_2} + y_2^2 a_2 \quad b = y_1 b_1 + y_2 b_2 \tag{3}$$

considering that species 2 is infinitely dilute in solvent 1 ($x_1 = 1$, $x_2 = 0$). In this model, the solute fugacity coefficient ϕ_2 is [24]

$$\ln \phi_2 = \ln\left(\frac{1}{1-b_1\rho}\right) + \frac{b_2\rho}{1-b_1\rho} - \frac{2\rho\sqrt{a_1 a_2}}{RT} - \ln Z \tag{4}$$

We use the following values of the pure component parameters that match the critical properties of each species with the vdW critical point: $a_{CO_2} = 3.658$ bar-(L/mol)^2, $b_{CO_2} = 0.0429$ L/mol, $a_{benzene} = 18.82$ bar-(L/mol)^2, $b_{benzene} = 0.1193$ L/mol, $a_{hexane} = 24.84$ bar-(L/mol)^2, and $b_{hexane} = 0.1744$ L/mol [25]. The compressibility factor Z is assumed known because it is a property of the pure solvent. The infinite-dilution low-density expansion of the fugacity coefficient is

$$\ln \phi_2^v = \sum_{n=1}^{\infty} \frac{n+1}{n} B_{n1} \rho^n - \ln Z \tag{5}$$

where B_{ij} is the mixture virial coefficient [24,26] corresponding to i molecules of species 1 and j molecules of species 2; the v superscript on ϕ indicates the values as given by the VEOS. Comparison of this series to an expansion of Eq. (4) for $\rho \to 0$ gives the mixture virial coefficients in terms of the vdW parameters

$$\begin{aligned} B_{11} &= \frac{1}{2}(b_1 + b_2) - \frac{\sqrt{a_1 a_2}}{RT} \\ B_{n1} &= \frac{1}{n+1}\left(b_1^n + n b_1^{n-1} b_2\right) \quad n > 1 \end{aligned} \tag{6}$$

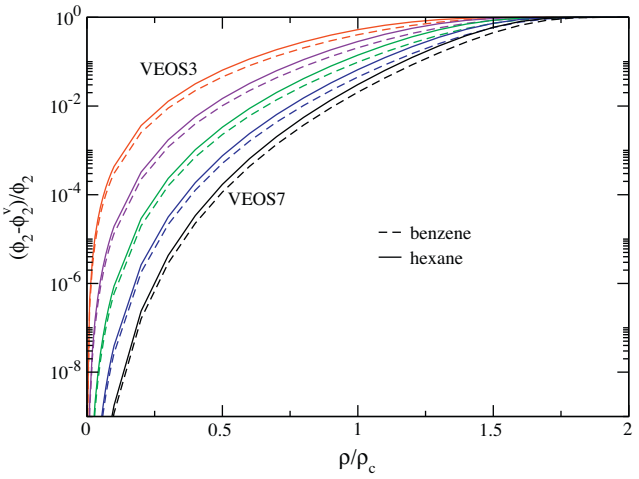

Fig. 1. The negative of the relative error in the VEOS*n* infinite-dilution solute fugacity coefficient for (a) benzene dissolved in CO_2 and (b) hexane dissolved in CO_2 as a function of the density reduced by the critical density of CO_2 at the critical temperature of CO_2. The exact behavior is assumed to be given by the vdW equation of state.

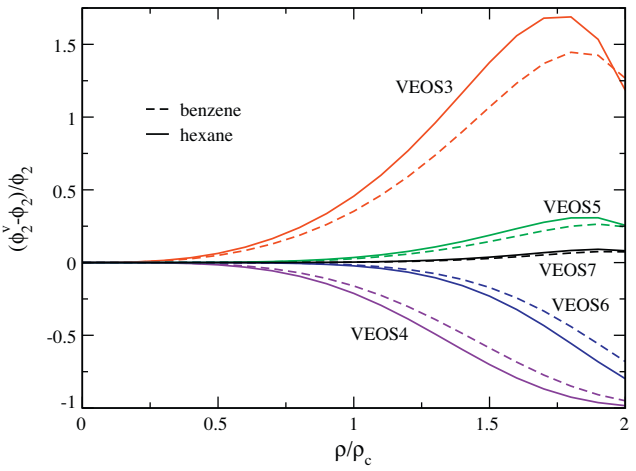

Fig. 2. Relative error in the VEOS*n* infinite-dilution solute fugacity coefficient for (a) benzene dissolved in CO_2 and (b) hexane dissolved in CO_2 as a function of the density reduced by the critical density of CO_2 at the critical temperature of CO_2. The exact behavior is assumed to be given by the SRK equation of state.

In Fig. 1, we plot the fractional error in the VEOS fugacity coefficient, given by the ratio of $\phi_2 - \phi_2^v$ to ϕ_2, with respect to reduced density for VEOS3 through VEOS7 at the critical temperature of CO_2, 304.13 K. As shown by Harvey, the error of ϕ_2^{VEOS3} for the CO_2–benzene mixture is significant (about 40%) at the critical density of CO_2, but each subsequent increase in order of the VEOS reduces the error at this density by about a factor of two. For VEOS7, the error is about 2%. At densities beyond the critical density, the VEOS approximation to the vdW EOS becomes increasingly poor and fails completely as ρ/ρ_c approaches 2. The fractional errors for each hexane VEOS*n* estimate are slightly worse than the respective benzene VEOSn estimate. One may consider that, with a larger vdW b value, hexane is larger than benzene, and thus could be solvated by more CO_2 molecules, making higher-order B_{n1} coefficients more relevant at a given density.

We next consider VEOS approximations for the same two mixtures as described by the SRK equation of state.

$$Z \equiv \frac{P}{\rho RT} = \frac{1}{1-b\rho} - \frac{\bar{a}\rho}{RT}\frac{\alpha(T)}{(1+b\rho)} \tag{7}$$

We employ expressions for the SRK parameters that match the critical properties of each species [24] with the SRK critical point

$$\begin{aligned} a &= \bar{a}\alpha(T) \\ \bar{a} &= 0.42748\frac{(RT_c)^2}{P_c} \\ \alpha(T) &= \left[1+\left(0.480+1.574\omega-0.176\omega^2\right)\left(1-\sqrt{\frac{T}{T_c}}\right)\right]^2 \\ b &= 0.08664\frac{RT_c}{P_c} \end{aligned} \tag{8}$$

We use the following values of the pure-component properties and parameters: $T_{c,CO_2} = 304.1$ K, $P_{c,CO_2} = 7380$ kPa, $\omega_{CO_2} = 0.239$, $T_{c,benzene} = 562.1$ K, $P_{c,benzene} = 4890$ kPa, $\omega_{benzene} = 0.212$, $T_{c,hexane} = 507.5$ K, and $P_{c,hexane} = 3010$ kPa, $\omega_{hexane} = 0.299$ [24]. The resulting values of the parameter b are notably smaller for each species than for the vdW EOS: $b_{CO_2} = 0.0297$ L/mol, $b_{benzene} = 0.0828$ L/mol, and $b_{hexane} = 0.1215$ L/mol.

Using the same Lorentz–Berthelot combining rules we did for vdW parameters (Eq. (3)), the fugacity coefficient, ϕ_2 is [24]

$$\begin{aligned} \ln\phi_2 = {} & \ln\left(\frac{1}{1-b_1\rho}\right) + \frac{b_2\rho}{1-b_1\rho} - \frac{2\sqrt{a_1a_2}}{RTb_1}\ln(1+b_1\rho) \\ & + \frac{a_1b_2}{RTb_1^2}\left[\ln(1+b_1\rho) - \frac{b_1\rho}{1+b_1\rho}\right] - \ln Z \end{aligned} \tag{9}$$

As before, we match terms from the density expansion of Eq. (9) with terms in Eq. (5) to determine expressions for virial coefficients in the limit of infinite dilution in terms of the SRK parameters

$$\begin{aligned} B_{n1} = {} & \frac{1}{n+1}\left[b_1^n + nb_1^{n-1}b_2\right] + (-1)^n\frac{b_1^{n-2}}{(n+1)RT} \\ & \times \left[2\sqrt{a_1a_2}b_1 + (n-1)a_1b_2\right] \quad n \geq 1 \end{aligned} \tag{10}$$

In Fig. 2, we plot the fractional error in the VEOS fugacity coefficient, given by the ratio of $\phi_2^v - \phi_2$ to ϕ_2, with respect to reduced density for VEOS3 through VEOS7 at the critical temperature of CO_2. Unlike the VEOS as applied to the vdW EOS, ϕ_2^v is sometimes too large and sometimes too small, but still converges to the correct result with enough terms. The error of ϕ_2^{VEOS3} for the mixtures is about 35% (similar to the vdW EOS) at the critical density of CO_2, but additional terms of the VEOS reduce the error more quickly than when applied to the vdW EOS, so that the error in VEOS7 is only 0.24%. This could be in part the result of the smaller b values and the characterization of molecular asymmetry through the acentric factor ω. The VEOS approximation to the SRK EOS continues working well up to very high density, with only 7% error in VEOS7 at $\rho/\rho_c = 2$.

While an exercise such as this can be helpful in setting expectations for the performance of the VEOS in characterizing supercritical fluid solubility, it is of course of interest to examine more sophisticated models. In the remainder of this work, we will do just that, considering the solubility of hexane in CO_2 while employing realistic molecular models of each for calculation of the mixture virial coefficients.

2.2. Molecular models

Our calculations employ the same molecular models examined by Cui et al. [27], who reported results from Gibbs-ensemble Monte Carlo (GEMC) simulations of model CO_2–hexane. Cui et al. con-

ducted their GEMC simulations in order to assess the adequacy of the models to describe solubility of hexane in CO_2 at supercritical conditions, as compared to experiments [28]. In the present analysis, we would like to gauge the ability of the VEOS to quantitatively describe the behavior of the models and their adequacy in describing the experimental system.

Hexane is modeled using the alkane potential proposed by Siepmann et al. [29], which is a flexible united-atom model based on Lennard-Jones interaction sites. Internal degrees of freedom include bond bending described by a harmonic bond-bending potential, and torsion with an associated dihedral potential. No bond stretching is permitted. Carbon dioxide is modeled using the EPM2 model of Harris and Yung [30], which is a rigid linear three-site model with point charges to model the electrostatics. The simulations of Cui et al. employed truncation of the potential with corrections applied for the neglected long-range interactions. It is notable that, in the present study, we have no need to introduce this feature, because our calculations are performed with an infinite simulation volume rather than with periodic boundary conditions, and, in principle, this creates a difference in the model we use versus the one examined by Cui et al. It seems unlikely that this variation will introduce effects that are larger than the difference in the way we use the models (GEMC versus VEOS), but we have not considered this question quantitatively.

2.3. Evaluation of virial coefficients for molecular models

The virial coefficients for a pure fluid are given in terms of cluster integrals involving interactions among n molecules for the coefficient B_n. The classical second virial coefficient is [9,26]

$$B_2(T) = -\frac{1}{2N_A V \Omega^2} \iint f_{12} e^{-\beta U_1} e^{-\beta U_2} dr_1 dr_2 d\boldsymbol{\omega}_1 d\boldsymbol{\omega}_2 \tag{11}$$

where $\beta = 1/kT$ with k the Boltzmann constant; N_A is Avogadro's number. The integral is performed over all positions $\mathbf{r}_1$ and $\mathbf{r}_2$ in a volume V, which is taken to be infinite. In practice we effect the division by V by holding the position of molecule 1 fixed. The symbols $\boldsymbol{\omega}_1$ and $\boldsymbol{\omega}_2$ represent all orientational and internal (conformation) coordinates of molecules 1 and 2, respectively, and $U_i(\boldsymbol{\omega}_i)$ is the intramolecular energy for molecule i. The integrals over $\boldsymbol{\omega}$ are normalized by dividing by $\Omega \equiv \int e^{-\beta U(\boldsymbol{\omega})} d\boldsymbol{\omega}$. Also, $f_{12} = \exp\left(-\beta u(r_1, r_2, \boldsymbol{\omega}_1, \boldsymbol{\omega}_2)\right) - 1$ is the Mayer function, where u is the total intermolecular energy between molecules 1 and 2. The mixture coefficients B_{20}, B_{11}, and B_{02} are all given by this integral, differing only in the choice of the species of the two molecules that are integrated upon. Expressions for higher-order coefficients B_n involve sums of integrals over n molecules, with the number of integrals growing rapidly with n [9].

Higher-order coefficients include "conformational" contributions that arise when dealing with flexible molecules [31,32], such as the model we employ here for hexane. These contributions take into account the fact that the set of conformations that a hexane molecule presents to another molecule (be it hexane or CO_2) is altered by the former's interactions with a third molecule. At the temperature we consider here we find that they are on the order of 1% for B_3 and 10% for B_4.

We use the Mayer-sampling Monte Carlo (MSMC) [16] method to evaluate the integrals that express the virial coefficients in terms of the molecular model. The technique is presented in detail in several places [12,16–21], and we will not repeat the description here. We will mention only that the method has the character of a Monte Carlo molecular simulation performed on i molecules of species 1 (CO_2) and j molecules of species 2 (hexane), for the evaluation of the coefficient B_{ij}. We employ the overlap-sampling implementation, using as a reference the integrals in the corresponding virial coefficient for hard spheres of diameter 6.93 Å when calculating pure hexane virial coefficients and 5 Å when calculating CO_2 or mixture coefficients (note that the choice of reference in principle has no effect on the results, and can be made within a broad range of values to help make the calculations more efficient). The MSMC technique used to evaluate the conformational contributions is new, and we will detail it in future work.

Virial coefficients were calculated from at least 10 independent MSMC simulations, each consisting of 3.5×10^7 equilibration steps followed by 10^9 steps of data collection. Confidence limits in the coefficients are based on the variance of the results from the independent simulations. More simulations were performed for B_{02} and B_{11} because of their large contribution to B_2, as well as for B_{04}, B_{13}, B_{22} and B_{31} due to increased difficulty in obtaining precise results for these coefficients. Ten separate simulations were also employed for each conformational contribution to each coefficient. CPU runtime for one 10^9-step simulation on one core of an Intel Core2 Quad Q550 2.83 GHz processor varied from 4 h for B_{20} to 13 h for B_{13}.

3. Results and discussion

We report components of the mixture coefficients B_2, B_3, and B_4 at 353.15 K, the temperature which Cui et al. obtained vapor–liquid coexistence data. The values are listed in Table 1. We observe that the precision of the calculations generally decreases with increasing number of hexane molecules in the coefficient.

We use these coefficients to obtain VEOS estimates of the chemical potentials μ_i of carbon dioxide and hexane in the vapor phase. From these μ_i, one can determine the range of conditions for which the vapor mixture is stable with respect to fluctuations in the number of molecules of species i, N_i:

$$\left(\frac{\partial \mu_1}{\partial N_1}\right)_{T,P,N_2} > 0 \tag{12}$$

which can be rewritten into a form more suitable for the VEOS [17,33]. The spinodal is the locus of points for which Eq. (12) is satisfied as an equality. Barring numerical problems or inadequacies in the model, the spinodal typically ends at a stable critical point where the following condition also holds

$$\left(\frac{\partial^2 \mu_1}{\partial N_1^2}\right)_{T,P,N_2} = 0 \tag{13}$$

The VEOS2-4 estimates of the spinodal line for the model CO_2–hexane system at 353.15 K are shown in the lower portion of Fig. 3.The line is presented against the vapor branch of the coexistence data determined by Cui et al. using Gibbs-ensemble Monte Carlo for the same model system as well as experimental measurements [28]. We do not have an alternative source to provide the true spinodal line, but we can see that the one given by the VEOS is compatible with the available data. The one point on this spinodal that we do know is the critical point at 353.15 K, which can be estimated from the maximum pressure in the coexistence envelope, roughly at $x_{CO_2} = y_{CO_2} = 0.93$, and $P = 10.5$ bar (this estimate-by-eye is indicated in Fig. 3 with a square). The VEOS3 and VEOS4 spinodal lines pass very near this point, but they do not terminate there: Eq. (13) is not satisfied for any point on each of the VEOS spinodals. We do note that for VEOS4 the second derivative given in Eq. (13) goes through a minimum (without crossing zero) along the spinodal curve at a somewhat higher pressure, the point $y_{CO_2} = 0.93$, $P = 12.2$ MPa labeled with an "x" in Fig. 3. We have found that such a "near-miss" critical point [17] can occur due to insufficient convergence of the VEOS, but it (i.e., the minimum) can still provide a reasonable indication of the location of the critical point. The VEOS2 spinodal appears to perform well at lower pressure (based on its proximity

Table 1
Mixture virial coefficients for the model CO_2–hexane system. B_{ij} is the coefficient for i molecules of CO_2 and j molecules of hexane. Numbers in parenthesis indicate 67% confidence limits in the last digit(s) of the reported value.

B_2 components (L/mol)		B_3 components (L/mol)^2		B_4 components (L/mol)^3	
B_{20}	−0.071473(2)	B_{30}	0.0024603(5)	B_{40}	0.0000382(2)
B_{11}	−0.258526(12)	B_{21}	0.008623(8)	B_{31}	0.000222(8)
B_{02}	−1.19608(12)	B_{12}	0.03373(7)	B_{22}	0.00144(5)
		B_{03}	−0.1554(4)	B_{13}	0.0111(5)
				B_{04}	−0.514(4)

to the higher-order spinodals), but deviates from the higher-order spinodals around 4 MPa.

Any attempt to locate the critical point using the VEOS must contend with the fact that the VEOS (or any classical model) has the wrong shape in the critical region [34,35], and it will inevitably fail to describe behavior here quantitatively without the application of special measures that account for the non-classical behavior [35]. Nevertheless, the VEOS has shown some success in providing an accurate location of the critical temperature and pressure of pure nonpolar fluids [12,22], albeit while consistently underestimating the critical density.

The solubility of hexane in CO_2 is given by the coexistence criteria for equality of temperature, pressure, and both species fugacities f_i between the hexane phase and the CO_2 phase. The present study provides a model for only the CO_2-rich phase, because this is the supercritical phase—the system temperature is 1.16 times the critical temperature of CO_2, and 0.70 times that of hexane. The hexane-rich phase has more of the character of a condensed liquid so we cannot expect the VEOS to provide a reasonable characterization of that side of the coexistence diagram. Instead, we treat this phase simply as an ideal solution, with each component fugacity given by $f_i = f_i^0 x_i$, where f_i^0 is a reference fugacity that is assumed

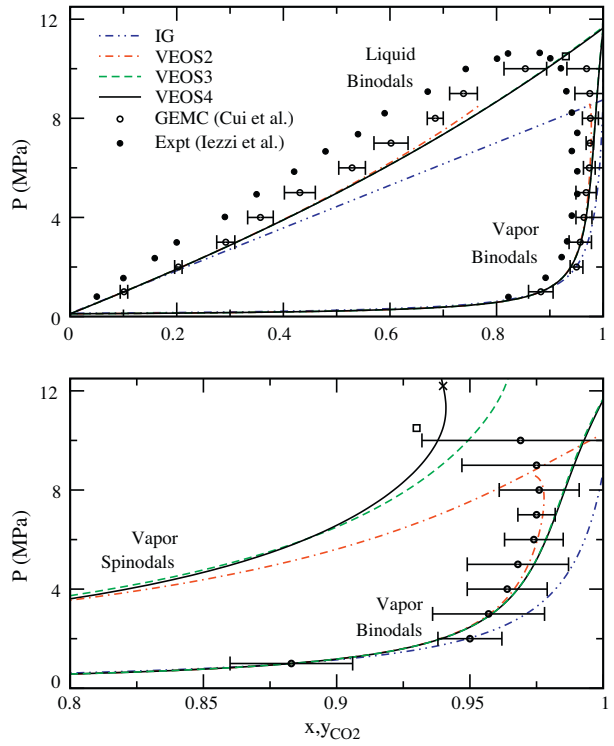

Fig. 3. Pressure-composition diagram for the system CO_2–hexane at 353.15 K. (Top) VEOS*n* estimates of both vapor and liquid coexistence curves are shown. (Bottom) Lines show VEOS*n* estimates of the vapor spinodals and VEOSn/ideal-mixture estimates of the vapor–liquid coexistence curve. Unfilled circles are GEMC simulation data [27] for the vapor–liquid coexistence curve, and filled circles are experimental data [30].

independent of pressure and composition, and x_i is the species-i mole fraction. Thus, to generate the estimated coexistence curves at a pressure P, we solve the equations

$$\begin{aligned} x_{CO_2} f^0_{CO_2} &= y_{CO_2} \phi^{VEOS}_{CO_2}(\rho, y_{CO_2}) P \\ (1 - x_{CO_2}) f^0_{hexane} &= (1 - y_{CO_2}) \phi^{VEOS}_{hexane}(\rho, y_{CO_2}) P \\ P &= P^{VEOS}(\rho, y_{CO_2}) \end{aligned} \tag{14}$$

for x_{CO_2}, y_{CO_2}, and ρ. We evaluate the reference fugacities using only the lowest-pressure (P = 1 MPa) GEMC binodal points, solving Eq. (14) instead for $f^0_{CO_2}$, f^0_{hexane}, and ρ using the GEMC values of x_{CO_2} and y_{CO_2} (0.10 and 0.88, respectively). We emphasize that this procedure is used only to establish a model for the liquid phase, and that the vapor is fully characterized by the VEOS.

The resulting binodal curves using VEOS2-4 as well as the ideal gas law (IG) for the CO_2-rich phase are also shown in Fig. 3. The ideal gas law underpredicts the solubility of hexane in CO_2 (in comparison to the GEMC data of Cui et al.) but provides a qualitative description of the phase behavior, especially at low pressures where the ideal-solution model parameters are fit. VEOS2 provides a substantial improvement over the ideal gas law, yielding a quantitatively accurate description of the vapor binodal up to 8.6 MPa, where VEOS2 predicts that the CO_2-rich phase becomes unstable. VEOS3 provides a better description of the vapor phase at high pressures, and the predicted binodal extends up to a pressure of 11.7 MPa, where the binodal curves intersect at $x_{CO_2} = 1$. This unphysical behavior of the binodals at higher pressures exists due to our application of the ideal-solution model well outside the region where it is parameterized; some improvement might be found through application of a Poynting correction to accommodate the pressure change, but we have not pursued this. The VEOS4 binodals deviate very little from VEOS3, even at high pressure, indicating that the virial equation has converged for the vapor conditions examined here. Given the ability of the VEOS estimates to reproduce the vapor branch of the GEMC data at moderate pressure, this treatment correctly indicates that the hexane solubility in the model supercritical mixture is too low in comparison to experiment [28], as noted by Cui et al. The predictions of the liquid binodals are less satisfactory, overpredicting the solubility of CO_2 above 3 MPa. Since the VEOS has converged, we must attribute this behavior to the (not unexpected) inadequacy of the ideal solution model to capture the full behavior of the liquid phase.

4. Conclusions

The description of supercritical fluids via the virial equation of state is a promising route to model the behaviors of importance to supercritical fluid applications. Interest in such an approach is greatly enhanced by the prospect of determining the model parameters from molecular considerations, via Mayer-sampling Monte Carlo using realistic transferable molecular force fields, or perhaps even results from *ab initio* computational chemistry calculations. The applications shown here indicate that such an approach holds significant promise. VEOS3 properties are converged at the conditions considered here, except for the very high pressures near the critical point. Given one set of points on the coexistence surface,

the vapor-phase binodal is obtained with quantitative accuracy up to about 8 MPa and provides the desired indication that the model hexane is too insoluble in the supercritical CO_2 in comparison to experiment. The weakest element of the demonstration is the crude ideal-solution treatment we apply for the subcritical phase. Often, practical applications can present more favorable situations for modeling the subcritical phase without requiring any points on the coexistence surface, such as in cases where a solid is dissolved in the supercritical fluid.

In the present application, we found that the VEOS by itself could not provide an appropriate representation of the critical region of the mixture. On the other hand, the spinodal seems to be well represented, and, through the near-miss critical criterion, the model does provide some indication of being in the vicinity of a critical point. It would of course be much more satisfactory were the model to provide a critical-point estimate that meets the true criteria of criticality, and moreover do so more accurately than the estimate given here. Given the well-known anomalies associated with the behavior of fluids near their critical point [34], we might not have expected so much, but we think with some development—perhaps connecting to ideas that bridge classical and non-classical critical-point behaviors [35]—it may be possible to improve the ability of the VEOS to provide reliable information about the critical region.

Acknowledgements

This work is supported by the National Science Foundation, Grants CHE-0626305 and CBET-0854340. Computational support was provided by the Open Science Grid, which is supported by the National Science Foundation and the US Department of Energy's Office of Science.

References

[1] C. Joslin, C. Gray, S. Goldman, B. Tomberli, W. Li, Solubilities in supercritical fluids from the virial equation of state, Molecular Physics 89 (1996) 489–503.
[2] D.A. Kofke, Getting the most from molecular simulation, Molecular Physics 102 (2004) 405–420.
[3] D.A. Kofke, Free energy methods in molecular simulation, Fluid Phase Equilibria 228–229 (2005) 41–48.
[4] D.A. Kofke, P.T. Cummings, Quantitative comparison and optimization of methods for evaluating the chemical potential by molecular simulation, Molecular Physics 92 (1997) 973–996.
[5] D.A. Kofke, P.T. Cummings, Precision and accuracy of staged free-energy perturbation methods for computing the chemical potential by molecular simulation, Fluid Phase Equilibria 150 (1998) 41–49.
[6] D.A. Kofke, D. Frenkel, Perspective:, Free energies and phase equilibria, in: S. Yip (Ed.), Handbook of Molecular Modeling, Kluwer Academic Publishers, Dordrecht, 2004.
[7] A.H. Harvey, On the suitability of the virial equation for modeling the solubility of solids in supercritical fluids, Fluid Phase Equilibria 130 (1997) 87–100.
[8] A.J. Perkins, The dissociation pressure of a solid under inert gas pressure, J. Chemical Physics 5 (1937) 180–185.
[9] J.P. Hansen, I.R. McDonald, Theory of Simple Liquids, 3rd ed., Academic Press, London, 2006.
[10] A.H. Ewald, W.B. Jepson, J.S. Rowlinson, The solubility of solids in gases, Discussions of the Faraday Society (1953) 238–243.
[11] B. Tomberli, S. Goldman, C. Gray, Predicting solubility in supercritical solvents using estimated virial coefficients and fluctuation theory, Fluid Phase Equilibria 187 (2001) 111–130.
[12] A.J. Schultz, D.A. Kofke, Sixth, seventh and eighth virial coefficients of the Lennard-Jones model, Molecular Physics 107 (2009) 2309–2318.
[13] L.G. MacDowell, C. Menduina, C. Vega, E. de Miguel, Critical properties of molecular fluids from the virial series, J. Chemical Physics 119 (2003) 11367–11373.
[14] L.G. MacDowell, C. Menduina, C. Vega, E. De Miguel, Third virial coefficients and critical properties of quadrupolar two center Lennard-Jones models, Physical Chemistry Chemical Physics 5 (2003) 2851–2857.
[15] B. Tomberli, S. Goldman, C. Gray, M. Saldaña, F. Temelli, Using solute structure to predict solubility of organic molecules in supercritical carbon dioxide, J. Supercritical Fluids 37 (2006) 333–341.
[16] J.K. Singh, D.A. Kofke, Mayer sampling: calculation of cluster integrals using free-energy perturbation methods, Physical Review Letters 92 (2004) 220601.
[17] A.J. Schultz, D.A. Kofke, Virial coefficients of Lennard-Jones mixtures, J. Chemical Physics 130 (2009) 224104.
[18] K.M. Benjamin, A.J. Schultz, D.A. Kofke, Gas-phase molecular clustering of TIP4P and SPC/E water models from higher-order virial coefficients, Industrial and Engineering Chemistry Research 45 (2006) 5566–5573.
[19] K.M. Benjamin, A.J. Schultz, D.A. Kofke, Virial coefficients of polarizable water: applications to thermodynamic properties and molecular clustering, J. Physical Chemistry C 111 (2007) 16021–16027.
[20] K.M. Benjamin, A.J. Schultz, D.A. Kofke, Fourth and fifth virial coefficients of polarizable water, J Physical Chemistry B 113 (2009) 7810–7815.
[21] K.M. Benjamin, J.K. Singh, A.J. Schultz, D.A. Kofke, Higher-order virial coefficients of water models, J. Physical Chemistry B 111 (2007) 11463–11473.
[22] A.J. Schultz, D.A. Kofke, Virial coefficients of model alkanes, J. Chemical Physics 133 (2010) 104101.
[23] K.R. Shaul, A.J. Schultz, D.A. Kofke, Mayer sampling Monte Carlo calculations of methanol virial coefficients, Molecular Simulation, in press.
[24] J.M. Prausnitz, R.N. Lichtenthaler, E.G. de Azevedo, Molecular Thermodynamics of Fluid-Phase Equilibria, Prentice-Hall, Englewood Cliffs, 1986.
[25] D.R. Lide, CRC Handbook of Chemistry and Physics, 89th ed. (Internet Version 2009), CRC Press/Taylor and Francis, Boca Raton, FL, 2008–2009.
[26] E.A. Mason, T.H. Spurling, The Virial Equation of State, Pergamon Press, Oxford, 1969.
[27] S.T. Cui, H.D. Cochran, P.T. Cummings, Vapor–liquid phase coexistence of alkane carbon dioxide and perfluoroalkane carbon dioxide mixtures, J. Physical Chemistry B 103 (1999) 4485–4491.
[28] A. Iezzi, P. Bendale, R.M. Enick, M. Turberg, J. Brady, 'Gel' formation in carbon dioxide – semifluorinated alkane mixtures and phase equilibria of a carbon dioxide – perfluorinated alkane mixture, Fluid Phase Equilibria 52 (1989) 307–317.
[29] J.I. Siepmann, S. Karaborni, B. Smit, Simulating the critical-behavior of complex fluids, Nature 365 (1993) 330–332.
[30] J.G. Harris, K.H. Yung, Carbon dioxide's liquid–vapor coexistence curve and critical properties as predicted by a simple molecular model, J. Physical Chemistry 99 (1995) 12021–12024.
[31] S. Caracciolo, B.M. Mognetti, A. Pelissetto, Virial coefficients and osmotic pressure in polymer solutions in good-solvent conditions, J. Chemical Physics 125 (2006) 094903–094908.
[32] S. Caracciolo, B.M. Mognetti, A. Pelissetto, Polymer size in dilute solutions in the good-solvent regime, J. Chemical Physics 125 (2006) 094904–094907.
[33] J.W. Tester, M. Modell, Thermodynamics and Its Applications, 3rd ed., Prentice Hall PTR, Upper Saddle River, NJ, 1997.
[34] H.E. Stanley, Introduction to Phase Transitions and Critical Phenomena, Oxford University Press, Oxford, 1971.
[35] M.A. Anisimov, J.V. Sengers, Critical region, in: J.V. Sengers, R.F. Kayser, C.J. Peters, H.J.J. White (Eds.), Equations of State for Fluids and Fluid Mixtures, International Union of Pure and Applied Chemistry, 2000.